



Cite this: *Phys. Chem. Chem. Phys.*, 2024, 26, 14186

## Size-dependent reactivity of $V_nO^+$ ( $n = 1-9$ ) clusters with ethane†

Hang Zhou,<sup>a</sup> Man Ruan,<sup>b</sup> Qing-Yu Liu,<sup>bc</sup> Yan-Xia Zhao,<sup>bc</sup> Rui-Yong Wang,<sup>id a</sup> Yuan Yang\*<sup>a</sup> and Sheng-Gui He <sup>id \*bcd</sup>

Cost-effective and readily accessible 3d transition metals (TMs) have been considered as promising candidates for alkane activation while 3d TMs especially the early TMs are usually not very reactive with light alkanes. In this study, the reactivity of  $V_n^+$  and  $V_nO^+$  ( $n = 1-9$ ) cluster cations towards ethane under thermal collision conditions has been investigated using mass spectrometry and density functional theory calculations. Among  $V_n^+$  ( $n = 1-9$ ) clusters, only  $V_{3-5}^+$  can react with  $C_2H_6$  to generate dehydrogenation products and the reaction rate constants are below  $10^{-13} \text{ cm}^3 \text{ molecule}^{-1} \text{ s}^{-1}$ . In contrast, the reaction rate constants for all  $V_nO^+$  ( $n = 1-9$ ) with  $C_2H_6$  significantly increase by about 2–4 orders of magnitude. Theoretical analysis evidences that the addition of ligand O affects the charge distribution of the metal centers, resulting in a significant increase in the cluster reactivity. The analysis of frontier orbitals indicates that the agostic interaction determines the size-dependent reactivity of  $V_nO^+$  cluster cations. This study provides a novel approach for improving the reactivity of early 3d TMs.

Received 28th February 2024,  
Accepted 19th April 2024

DOI: 10.1039/d4cp00857j

rsc.li/pccp

## Introduction

Alkanes are highly abundant in nature and constitute the primary components of natural gas and crude oil, serving as essential raw materials for the chemical industry.<sup>1</sup> However, due to the robust thermodynamic nature of the C–H bond, its activation presents a considerable challenge.<sup>2</sup> Consequently, investigating the mechanisms of C–H bond activation is of great significance in the development of better performing catalysts for alkane transformation.<sup>3</sup> The investigation of the reactions between gas-phase atomic clusters with alkane molecules is regarded as a crucial approach to comprehending the mechanisms of C–H activation at the molecular level.

Numerous studies have been documented on the activation and conversion of alkanes by gas-phase metal clusters. There has been a predominant focus on the investigation of noble metal clusters. For example, the previous investigations have

shown that  $Pt_n^+$  ( $n \leq 9$ ),<sup>4-7</sup>  $Pd_n^+$  ( $n = 2$  and  $3$ ),<sup>8</sup>  $Rh_n^+$  ( $n = 1-30$ ),<sup>9</sup>  $Os^+$ ,<sup>10,11</sup> and  $Ir^{+12,13}$  exhibit notable reactivity in dehydrogenation of light alkanes. Additionally, neutral clusters such as  $Pd_n$  ( $n \leq 23$ )<sup>14</sup> and  $Pt_n$  ( $n \leq 24$ ),<sup>15</sup> and the anionic clusters such as  $Rh_n^-$  ( $n \leq 10$ ),<sup>16</sup>  $Rh_nC_{20}H_{10}^-$  ( $n = 4-7$ ),<sup>17</sup> and  $Pt_n^-$  ( $n \leq 7$ )<sup>6</sup> have been demonstrated to have highly size-selective patterns in the activation of the C–H bond in methane. In contrast, the studies on alkane C–H activation by base metals are very limited. The reactions of the clusters of 5d base metals  $Ta^{18-23}$  and  $W^{24-27}$  with methane have been reported. Although 3d transition metals (TMs) are more abundant and economically accessible compared to 5d TMs, studies on alkane C–H activation by 3d TMs, especially the early 3d TMs, are very limited. The studies conducted by Armentrout *et al.* demonstrated that  $V^+$  is inactive with  $CH_4$ .<sup>28</sup> In a previously documented study involving the reaction of  $Ta_xO^+$  ( $x = 4$  and  $5$ ) with methane,<sup>20</sup> it was observed that the incorporation of the ligand O into the metal clusters markedly enhanced the cluster reactivity. In a subsequent investigation of methane activation by tungsten species,<sup>24</sup> it was noted that  $W_n^+$  ( $n \geq 2$ ) exhibited minimal reactivity, while the addition of O significantly promoted  $CH_4$  dehydrogenation. These observations prompted us to explore methodologies for improving the reactivity of 3d TM clusters with light alkanes by doping oxygen atoms.

In this study, the reactivity of  $V_n^+$  and  $V_nO^+$  ( $n = 1-9$ ) with ethane was investigated using a combination of time-of-flight mass spectrometry and quantum chemical calculations. It was observed that the reactivity of vanadium cluster cations toward ethane can be significantly enhanced with the addition of O

<sup>a</sup> Henan Key Laboratory of Crystalline Molecular Functional Materials, College of Chemistry, Zhengzhou University, Zhengzhou 450001, P. R. China.

E-mail: yangy@zzu.edu.cn

<sup>b</sup> State Key Laboratory for Structural Chemistry of Unstable and Stable Species, Institute of Chemistry, Chinese Academy of Sciences, Beijing 100190, P. R. China.

E-mail: shengguihe@iccas.ac.cn

<sup>c</sup> Beijing National Laboratory for Molecular Sciences and CAS Research/Education Centre of Excellence in Molecular Sciences, Beijing 100190, P. R. China

<sup>d</sup> University of Chinese Academy of Sciences, Beijing 100049, P. R. China

† Electronic supplementary information (ESI) available: Additional experimental and theoretical results (data analysis, DFT calculated structures and reaction mechanisms). See DOI: <https://doi.org/10.1039/d4cp00857j>

ligands, affirming the modulating effect of O on the reactivity of early 3d TMs. Insights into improving the catalytic activity of these metals are thus provided. Note that the reaction of  $V_n^+$  ( $n = 1-9$ ) with  $H_2O$  has been experimentally investigated in the literature.<sup>29</sup>

## Methods

### Experimental methods

A laser ablation method was used to generate the  $V_n^+$  and  $V_nO^+$  cations through the irradiation of a focused pulsed laser beam (532 nm, 5–8 mJ, 10 Hz) onto a rotating and translating V disk in the presence of 4 atm He carrier gas. The cluster cations of interest,  $V_n^+$  ( $n = 1-9$ ) and  $V_nO^+$  ( $n = 1-9$ ), were mass-selected using a quadrupole mass filter (QMF)<sup>30</sup> and then introduced into the linear ion trap (LIT)<sup>31</sup> reactor. After thermalization by collisions with a pulse of cooling gas He (3 Pa), the cluster ions reacted with a pulse of  $C_2H_6$  seeded in He gas for about 2 ms. The temperature of the cooling gas, the reactant gas ( $C_2H_6$ ), and the LIT reactor was around 298 K. The masses and abundances of the reactant and product cations were detected using a home-made reflection time-of-flight mass spectrometer (TOF-MS).<sup>32</sup>

### Computational methods

Density functional theory (DFT) calculations by using the Gaussian 09 program<sup>33</sup> were carried out to investigate the structures of  $V_n^+$  and  $V_nO^+$  ( $n = 1-9$ ) cations, as well as the reaction mechanisms of  $V_n^+$  ( $n = 2$  and 3) and  $V_nO^+$  ( $n = 1, 2$ , and 3) with  $C_2H_6$ . The benchmark calculations showed that the BPBE functional<sup>34,35</sup> generally performed best for the bond energy of V–V, V–C, V–O, V–H, C–H, and H–H compared with the experimental values (Table S1, ESI†). Thus, the BPBE functional was adopted in this work. For all the calculations, the TZVP basis sets<sup>36</sup> were used for all of the elements (C, H, O, and V). A Fortran code based on a genetic algorithm<sup>37</sup> was used to generate initial guess structures of  $V_n^+$  ( $n = 7-9$ ) and  $V_nO^+$  ( $n = 5-9$ ) clusters. Reaction mechanism calculations involved the geometric structures of reaction intermediates (IMs) and transition states (TSs) that were optimized and vibrational frequencies were calculated to check that each of the IMs and TSs has zero or only one imaginary frequency. The TSs were optimized using the Berny algorithm method.<sup>38</sup> The initial guess structures of the TS species were obtained through relaxed potential energy surface scans using single or multiple internal coordinates. Intrinsic reaction coordinate calculations<sup>39</sup> were conducted to make sure that a TS connects two appropriate IMs. The zero-point vibration-corrected energies ( $\Delta H_0$ ) in eV are reported in this work. The natural bond orbital (NBO) analysis was performed with the software NBO 5.9.<sup>40</sup>

## Results

### Experimental results

In general, a sharp contrast in reactivity difference of pure vanadium cluster cations *versus* vanadium oxide cluster cations with ethane was observed (Fig. S1, ESI†):  $V_n^+$  with  $n = 2-5$  can

lead to the dehydrogenation reaction or adsorption reaction with ethane. However, with the introduction of one oxygen atom, all  $V_nO^+$  ( $n = 1-9$ ) can generate adsorption/dehydrogenation product ions with ethane. The typical TOF mass spectra for the reactions of mass-selected  $V_n^+$  and  $V_nO^+$  ( $n = 1-4$ ) with  $C_2H_6$  are shown in Fig. 1. When  $V^+$  interacts with 0.89 Pa  $C_2H_6$  for about 2 ms, no new product peaks were observed relative to the background peak generated from the reaction with water impurity. As the cluster size of  $V_n^+$  increases, weak cluster reactivity can be observed. Fig. 1(b2) shows that in the reaction between  $V_2^+$  and 0.47 Pa  $C_2H_6$  for 2 ms, a very weak product peak ( $V_2C_2H_6^+$ ) for adsorbing a single  $C_2H_6$  molecule appeared. When the cluster upsizes to  $V_3^+$  and  $V_4^+$ , the dehydrogenation products of  $V_3C_2H_2^+$  and  $V_4C_2H_{2,4}^+$  were observed in Fig. 1(b3) and (b4). In contrast to the case of  $V_n^+$ , the reactivity of  $V_nO^+$  with  $C_2H_6$  was greatly improved. As demonstrated in Fig. 1(d1) and (d3),  $V_{1,3}O^+$  were able to produce the adsorption products. In the reaction system of  $V_{2,4}O^+$ , more than half of the initial reactant ions were converted to dehydrogenation product ions at low pressure of  $C_2H_6$  ( $\leq 0.02$  Pa, Fig. 1(d2) and (d4)). In addition, a relatively weak signal that can be assigned to  $V_2OH_2^+$  appears in the reaction of  $V_2O^+$  with  $C_2H_6$ , corresponding to the loss of a  $C_2H_4$  molecule ( $V_2O^+ + C_2H_6 \rightarrow V_2OH_2^+ + C_2H_4$ ).

The rate constants ( $k_1$ ) for the pseudo-first-order reactions of  $V_n^+$  and  $V_nO^+$  ( $n = 1-9$ ) with  $C_2H_6$  were estimated using the following equation:

$$\ln \frac{I_R}{I_T} = -k_1 \frac{P}{k_B T} t_R$$

in which  $I_R$  is the intensity of reactant cluster ions after the reaction,  $I_T$  is the total ion intensity including the product ion contribution except for water adsorption,  $P$  is the effective pressure of the reactant gas,  $k_B$  is the Boltzmann constant,  $t_R$  is the reaction time, and  $T$  is the temperature of the reactant gas. The  $k_1$  values for the reactions of  $V_{2-5}^+$  and  $V_{1-9}O^+$  with  $C_2H_6$  were determined (Fig. S2, S3 ESI† and Table 1) and are shown in Fig. 2 as a function of the cluster size. For the  $V_n^+$  system, triatomic  $V_3^+$  has a slightly smaller  $k_1$  than diatomic  $V_2^+$ . The  $k_1$  values of  $V_n^+$  ( $n = 3-5$ ) +  $C_2H_6$  increased with the increase of the cluster size, and the highest reactivity was observed for  $V_5^+$ . This result is consistent with the highest reactivity of  $V_5^+$  in the reaction of  $V_n^+$  with  $H_2O$ , which was explained with the synergistic effect of three V atoms.<sup>29</sup> In sharp contrast, for each of the  $n$  values, the  $V_nO^+$  cluster is more reactive than  $V_n^+$  by two or more orders of magnitude and exhibits a completely different reactivity variation with respect to the cluster size. Among the  $V_nO^+$ , the reaction couple  $V_2O^+/C_2H_6$  has the largest  $k_1$  of  $1.49 \times 10^{-9} \text{ cm}^3 \text{ molecule}^{-1} \text{ s}^{-1}$ . The  $k_1$  values of  $VO^+$  and  $V_3O^+$  are smaller than that of  $V_2O^+$ . When the cluster upsizes, the reactivities of  $V_nO^+$  decline, and the  $k_1$  values gradually decrease from  $2.01 \times 10^{-10} \text{ cm}^3 \text{ molecule}^{-1} \text{ s}^{-1}$  for  $n = 4$  to  $2.94 \times 10^{-13} \text{ cm}^3 \text{ molecule}^{-1} \text{ s}^{-1}$  at  $n = 9$ . The reactivity comparison of  $V_n^+$  and  $V_nO^+$  ( $n = 1-9$ ) cluster cations indicates that oxygen atoms play a crucial role in modulating the reactivity of the vanadium cluster cations. The doping of the O atom is particularly significant in enhancing the metal cluster reactivity.

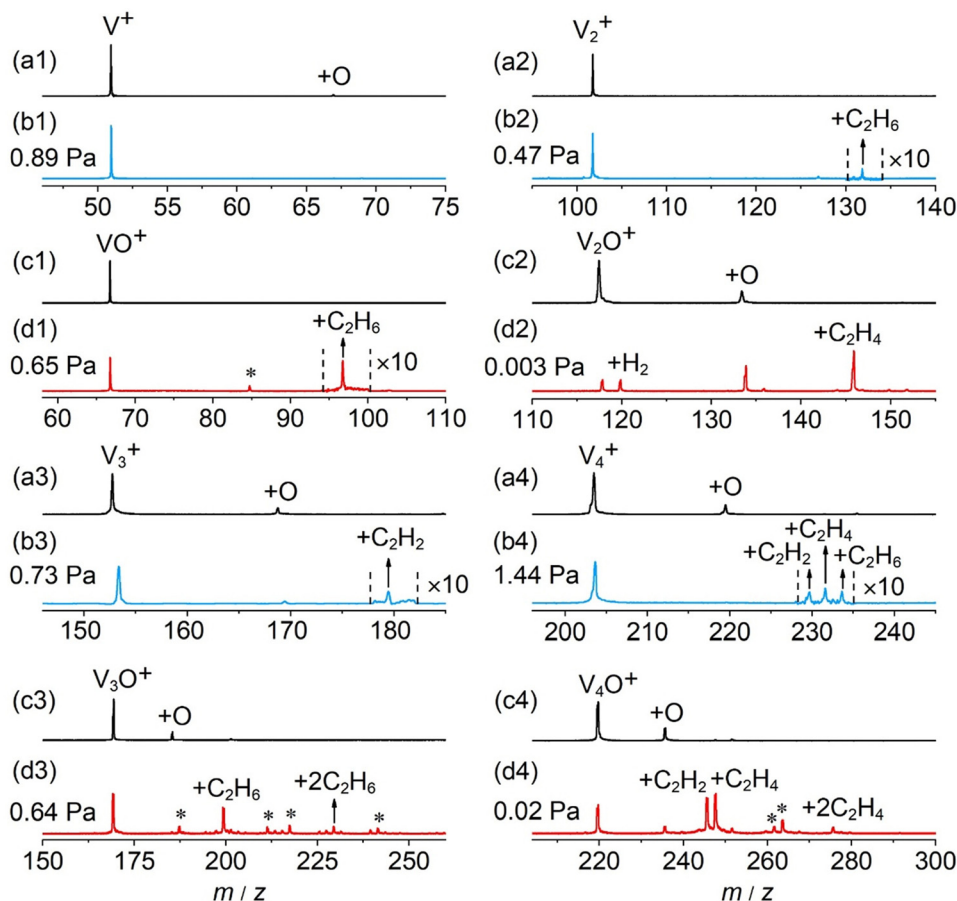


**Fig. 1** TOF mass spectra for the reactions of mass-selected  $V^+$  (a1),  $VO^+$  (c1),  $V_2^+$  (a2),  $V_2O^+$  (c2),  $V_3^+$  (a3),  $V_3O^+$  (c3),  $V_4^+$  (a4), and  $V_4O^+$  (c4) cations with  $C_2H_6$ . The pressures of  $C_2H_6$  are shown. The reaction times are around 2 ms. The peaks marked with asterisks originated from water impurities. The  $V_nX^+$  and  $V_nOX^+$  ( $X = C_2H_2, C_2H_4$ , etc.) species are labeled as +X.

**Table 1** Rate constants ( $k_1$ ,  $cm^3$  molecule $^{-1}$  s $^{-1}$ ) for the reaction of  $V_n^+$  and  $V_nO^+$  with  $C_2H_6$

Cation	$k_1$ , $C_2H_6$	Cation	$k_1$ , $C_2H_6$
$V^+$	—	$VO^+$	$3.33 \times 10^{-13}$
$V_2^+$	$1.13 \times 10^{-13}$	$V_2O^+$	$1.49 \times 10^{-9}$
$V_3^+$	$8.55 \times 10^{-14}$	$V_3O^+$	$2.14 \times 10^{-12}$
$V_4^+$	$1.32 \times 10^{-13}$	$V_4O^+$	$2.01 \times 10^{-10}$
$V_5^+$	$4.04 \times 10^{-12}$	$V_5O^+$	$1.50 \times 10^{-10}$
$V_6^+$	—	$V_6O^+$	$7.28 \times 10^{-11}$
$V_7^+$	—	$V_7O^+$	$1.49 \times 10^{-11}$
$V_8^+$	—	$V_8O^+$	$1.85 \times 10^{-12}$
$V_9^+$	—	$V_9O^+$	$2.94 \times 10^{-13}$

### Computational results

The global minimum structures of  $V_n^+$  and  $V_nO^+$  ( $n = 1-9$ ) clusters from the DFT calculations are shown in Fig. 3 and Fig. S4–S8 (ESI $^+$ ). Most of the lowest-lying isomers are consistent with structures calculated with the BP86 method in the literature, except  $V_6^+$  and  $V_{2,9}O^+$ .<sup>29</sup> For a deeper understanding of the differences in reactivity between  $V_n^+$  and  $V_nO^+$ , the reaction pathways of  $n = 1-3$  reaction systems were calculated using the DFT method and the results for  $V_2^+$  and  $V_2O^+$  cations

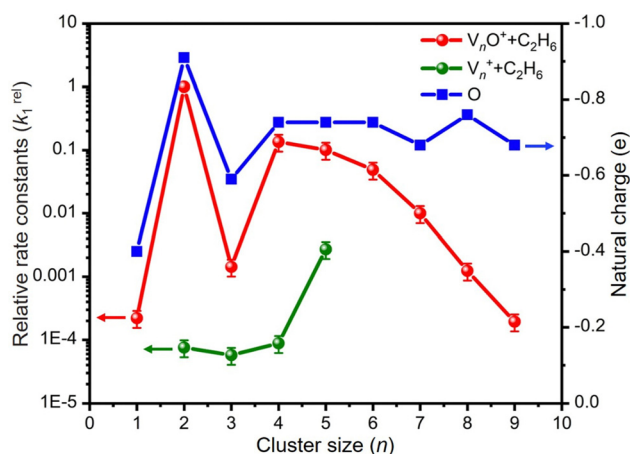


**Fig. 2** Relative rate constants ( $k_1^{rel}$ ) for the reactions of  $V_n^+$  and  $V_nO^+$  ( $n = 1-9$ ) with  $C_2H_6$ . The  $k_1^{rel}$  values are relative to the absolute rate constant  $k_1(V_2O^+ + C_2H_6) = 1.49 \times 10^{-9}$   $cm^3$  molecule $^{-1}$  s $^{-1}$ . The uncertainties (within 30%) of  $k_1^{rel}$  values are shown. The uncertainties of the absolute  $k_1$  values are within factors of 2–3. The variations of natural charges (e) of oxygen atoms in  $V_nO^+$  clusters are also shown for understanding the relative activity.

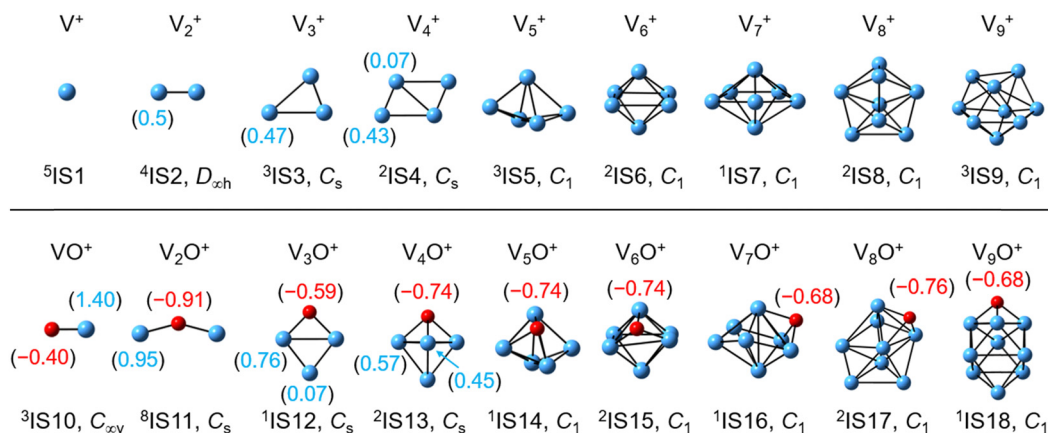


Fig. 3 DFT-optimized most stable structures of the  $V_n^+$  and  $V_nO^+$  ( $n = 1-9$ ) clusters at the BPBE level. The point group is given under each structure. The superscripts indicate the spin multiplicities. The natural charge (e) of the V atoms and O atoms is shown in parentheses.

with  $C_2H_6$  are shown in Fig. 4. When a  $C_2H_6$  molecule approaches the  $V_2^+$  cation, an encounter complex is formed with a binding energy of 0.42 eV ( $^4I1$ ). The subsequent step for

the activation of the first C–H bond involves a spin flip from quartet to doublet states (Fig. S9a, ESI<sup>†</sup>). Since the energy of  $^2TS1$  is 0.15 eV higher than those of the separated reactants, the

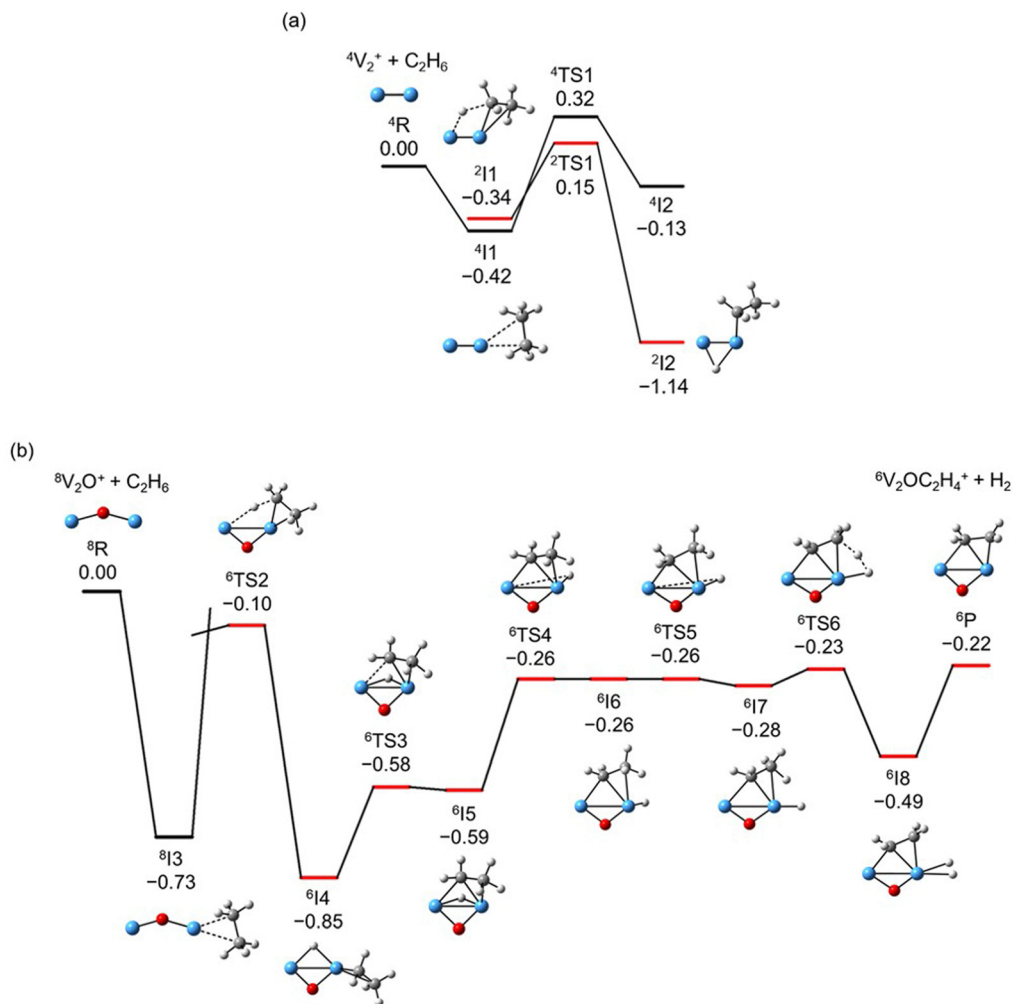


Fig. 4 DFT calculated potential energy profiles for the reactions of  $V_2^+$  and  $V_2O^+$  with  $C_2H_6$ . Relative energies of the reaction intermediates (I1–I8), transition states (TS1–TS6), and products (P) with respect to the separated reactants ( $V_2O_{0,1}^+ + C_2H_6$ ) are given in eV ( $\Delta H_0$ ). The superscripts indicate spin multiplicities.

process of C–H cleavage initiated by  $V_2^+$  is kinetically unfavorable under thermal collision conditions. The  $V_2C_2H_6^+$  weakly observed in the experiment (Fig. b2) is thus an adsorption product and the C–H bond is not cleaved. In contrast to the inertness of  $V_2^+$  in cleaving the C–H bond,  $V_2O^+$  can react with  $C_2H_6$  to form the dehydrogenation product  $V_2OC_2H_4^+$ . In  $V_2O^+ + C_2H_6$ , the V atom captures  $C_2H_6$  with a binding energy of 0.73 eV to form the complex  ${}^8I3$ . The breaking of the first C–H bond proceeds through a mechanism of synergistic activation by the V–V metal bond involving a spin crossing process (octet  $\rightarrow$  sextet, Fig. S9b, ESI $^\dagger$ ), resulting in the formation of the lowest energy intermediate  ${}^6I4$  with a four-membered –V–H–V–O–ring and a three-membered –C–C–V–ring. The transition from  ${}^8I3$  to  ${}^6I4$  is kinetically favorable since TS2 has energy lower than that of the isolated reactants by 0.1 eV. Then, the  $C_2H_5$  moieties in  ${}^6I4$  moves towards another V atom, resulting in the formation of a new V–C bond in  ${}^6I5$ . After a structural rearrangement to break the V–H bond in  ${}^6I5$ , the second C–H bond can be cleaved. The resulting intermediate  ${}^6I8$  has enough internal energy to evaporate the  $H_2$  unit to produce the experimentally observed  $V_2OC_2H_4^+$  product ion.

The systems of  $V_nO_m^+$  ( $n = 1$  and  $3$ ;  $m = 0$  and  $1$ ) involving the first C–H bond cleavage, which is generally viewed as the rate limiting step in alkane conversion, were also considered. As shown in Fig. 5, the oxidative addition of the C–H bond of  $C_2H_6$  by the cluster systems of  $V_{1-3}^+$  encounters the energy barriers in the range of  $-0.03$ – $0.15$  eV. Note that the direct evaporation of

the  $C_2H_6$  from adsorption intermediates (I1, I9, and I13) is an entropically more favorable process, which is in good agreement with the experimental results that only very weak adsorption/dehydrogenation products could be observed. In sharp contrast, the C–H bond cleavage of  $C_2H_6$  mediated by  $V_{1-3}O^+$  experiences a significantly negative energy barrier ( $\leq -0.1$  eV). For the  $VO^+/C_2H_6$  system, the V atom readily traps the  $C_2H_6$  molecule and releases 1.00 eV energy ( ${}^3I11$ ). Then, the C–H bond is inserted by the V atom accompanied by a spin flip from triplet to singlet states ( ${}^3I11 \rightarrow {}^1TS8$ ). The energy of the formed intermediate  ${}^1I12$  ( $\Delta H_0 = -0.37$  eV) closely approximates that of the transition state  ${}^1TS8$  ( $\Delta H_0 = -0.35$  eV), facilitating an almost barrierless transition from I12 back to I11. Although  ${}^3I11$  can dissociate back to the separated reactants ( ${}^3I11 \rightarrow VO^+ + C_2H_6$ ), a small portion of I11 may be stabilized through the collisions with the bath gas, resulting in the observation of the weak adsorption product  $VOC_2H_6^+$  in the experiment (Fig. d1). In contrast, the intermediates (I4–I8) and transition states (TS3–TS6) along the reaction pathway of  $V_2O^+/C_2H_6$  are much lower in energy than the TS2 state (Fig. 4). Once intermediate I4 is formed, it has more chance to form I8 that can dissociate into  $V_2OC_2H_4^+ + H_2$  ( ${}^6P$ ), which is consistent with the experimental observation that  $V_2O^+$  reacts much faster than  $VO^+$  (Fig. 2). For the system of  $V_3O^+/C_2H_6$ , considering the low energy barrier of C–H activation ( $-0.31$  eV), I16 shows a higher tendency than I4 to proceed back to the adsorption intermediate (I15) and decompose to the  $V_3O^+ + C_2H_6$  under

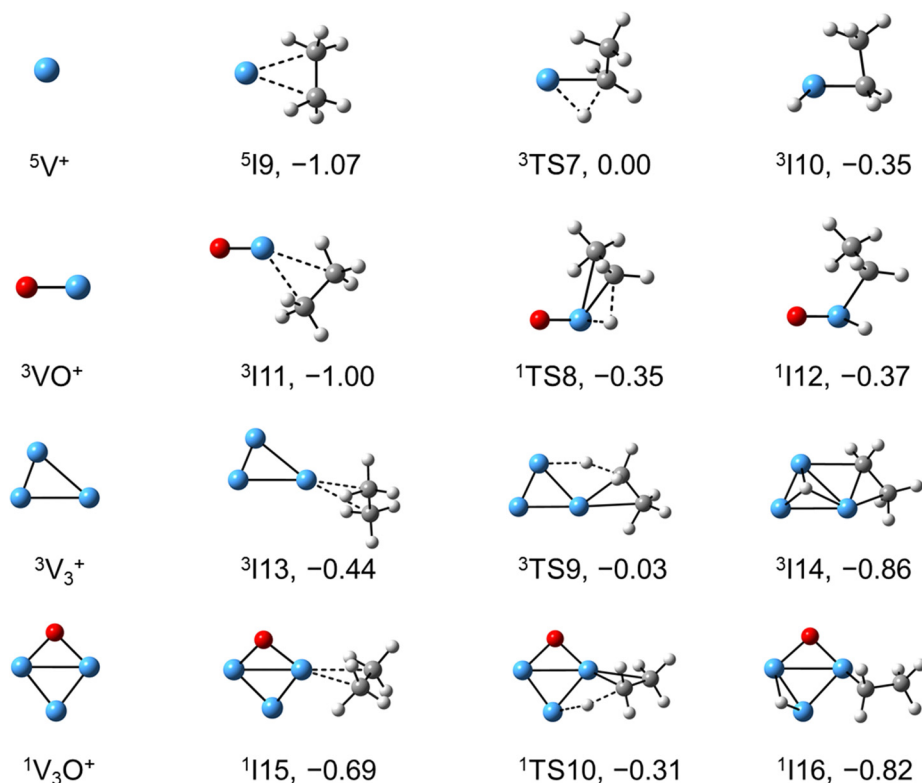


Fig. 5 DFT calculated the structures of  $V_n^+$  and  $V_nO^+$  ( $n = 1, 3$ ) isomers, reaction IMs, and transition states for the first C–H bond activation of ethane. The relative energies with respect to the separated reactants ( $V_{1,3}O_{0,1}^+ + C_2H_6$ ) are given in eV ( $\Delta H_0$ ).

entropy-driven conditions, which rationalizes the lower reaction rate of  $V_3O^+ + C_2H_6$  than that of  $V_2O^+ + C_2H_6$  in the experiment (Fig. 2).

## Discussion

Reactions involving atomic metal ions and the corresponding oxide species with alkanes have been extensively documented,<sup>41–52</sup> whereas the oxo-ligand effect of polyatomic metal species has received limited attention. Eckhard *et al.* performed a comparative study on the reactions of  $CH_4$  with  $Ta_x^+$  and  $Ta_xO^+$  ( $x = 4$  and  $5$ ) clusters.<sup>20</sup> It has been demonstrated that the doped oxygen atom does not directly participate in the reaction. Instead, it modifies the local electronic charge distribution of the tantalum clusters that appears to be favorable for C–H bond activation through a metal insertion mechanism. Given the previous proposals, we conducted a comparison of the charge changes of atoms in the  $V_n^+$  and  $V_nO^+$  systems. In the literature, the C–H cleavage involves electron transfer from the occupied orbitals of alkane to the metal empty orbitals. The amount of positive charges within the cluster will determine its reactivity towards the alkane. According to the NBO analysis shown in Fig. 3, the high electron-withdrawing capability of the O atom significantly increases the positive charge on V atoms in  $V_nO^+$  systems. Consequently, the  $V_nO^+$  clusters can have much higher reactivity than the  $V_n^+$ . For  $V_nO^+$  cluster systems, the V atom adjacent to the O atom serves as the adsorption site for  $C_2H_6$  and as reactive sites to bring about C–H activation. The accumulation of large amounts of positive charges in V induced by oxygen is the crucial factor to profoundly affect the cluster reactivity. In other words, a striking correlation between the negative charge on O atom and  $k_1$  values emerges as shown in Fig. 2 and 3.  $V_2O^+$  with the most negative charge ( $-0.91e$ ) on O among  $V_{1-3}O^+$  exhibits the highest reactivity. The oxygen in  $VO^+$  carries the least negative charge ( $-0.40e$ ), resulting in its lowest reactivity. However, the reactivity of  $V_{4-9}O^+$  clusters decreases with the increase of the cluster size, while the negative charge on the O atom almost maintains a constant value ( $-0.68$  to  $-0.74e$ ). This could be attributed to the more crowded steric structure, which hinders the activation of the C–H bond.

In transition-metal-catalyzed organic reactions, agostic interaction is commonly defined as the intramolecular interaction between the hydrogen atom of a C–H bond with a nearby metallic center, which plays a crucial role in C–H bond activation.<sup>53–56</sup> In such interaction, the  $\sigma(C-H)$  orbital (alkane HOMO) acts as a donor orbital, whereas the acceptor orbitals could be empty molecular orbitals (cluster LUMO) of metal species.<sup>57–59</sup> The smaller energy gap helps to form stronger agostic interaction, enhancing the electron transfer to activate the C–H bond. Therefore, to further explore the effect of the oxygen ligand on the reactivity of metal clusters of different sizes, we analyzed the orbital interactions between  $V_nO^+$  and  $C_2H_6$  during the reactions (*e.g.*,  $V_3O^+/C_2H_6$  couple in Fig. S10, ESI†) and the HOMO of  $C_2H_6$  and the LUMO of  $V_nO^+$  ( $n = 1-9$ ) cations are shown in Fig. 6. For  $V_nO^+$  with small cluster sizes ( $n = 1-3$ ), the energy gap of  $V_2O^+$  (LUMO)  $\leftrightarrow$   $C_2H_6$  (HOMO) is

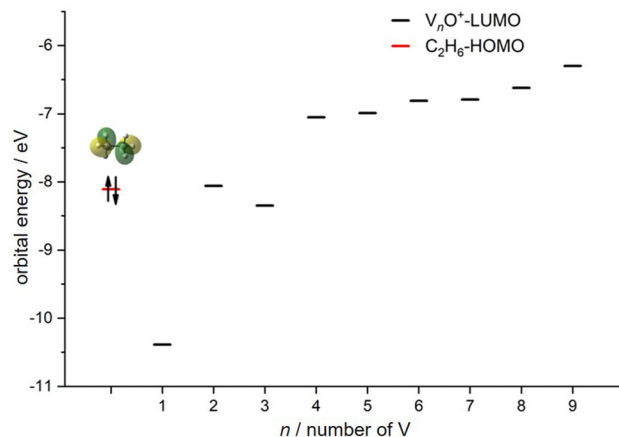


Fig. 6 HOMO levels of  $C_2H_6$  and LUMO levels of  $V_nO^+$  ( $n = 1-9$ ) cations. The up and down arrows denote  $\alpha$  and  $\beta$  electrons, respectively.

smaller compared to that of  $VO^+$  and  $V_3O^+$ , leading to the strongest agostic interaction and the fastest reaction rate for the  $V_2O^+/C_2H_6$  couple (Fig. 2). In contrast, the slowest reaction rate of  $VO^+$  with  $C_2H_6$  can be attributed to the largest energy gap of  $VO^+$  (LUMO)  $\leftrightarrow$   $C_2H_6$  (HOMO). For the  $V_nO^+$  clusters with larger sizes ( $4 \leq n \leq 9$ ), the energy gap increases as the cluster is upsized, resulting in weaker and weaker agostic interactions, which is consistent with the rate constant decrease of  $V_nO^+$  with  $C_2H_6$  from  $n = 4$  to  $n = 9$  (Fig. 2).

## Conclusion

The reactions of ethane with vanadium cluster cations  $V_n^+$  ( $n = 1-9$ ) and their corresponding oxide systems  $V_nO^+$  ( $n = 1-9$ ) have been comparatively studied *via* mass-spectrometry-based experiments. The O atom doped vanadium clusters are much more reactive than the non-doped  $V_n^+$  ones. The reactivity of  $V_2O^+$  is enhanced by four orders of magnitude with respect to that of  $V_2^+$  and  $V_2O^+$  is also the most reactive cluster among  $V_nO^+$  clusters ( $n = 1-9$ ). The mechanistic studies reveal that the reactivity of  $V_nO^+$  clusters is enhanced by the modification of charge distribution within the cluster through the introduction of oxygen atoms. The agostic interaction to interpret the size-dependent reactivity of  $V_nO^+$  has been proposed. This study not only extends our understanding of C–H activation of light alkanes (ethane) by metal systems but also provides insights into doping of O atoms to enhance the reactivity of early 3d transition metals.

## Conflicts of interest

There are no conflicts to declare.

## Acknowledgements

This work was financially supported by the National Natural Science Foundation of China (No. 22203078, 92161205, 22121002, and 22322307), the Youth Innovation Promotion

Association CAS (No. 2018041), and the China Postdoctoral Science Foundation (No. 2022TQ0289).

## References

- 1 Y. Wang, P. Hu, J. Yang, Y.-A. Zhu and D. Chen, *Chem. Soc. Rev.*, 2021, **50**, 4299–4358.
- 2 X.-S. Xue, P. Ji, B. Zhou and J.-P. Cheng, *Chem. Rev.*, 2017, **117**, 8622–8648.
- 3 Y. Liu, J.-C. Liu, T.-H. Li, Z.-H. Duan, T.-Y. Zhang, M. Yan, W.-L. Li, H. Xiao, Y.-G. Wang, C.-R. Chang and J. Li, *Angew. Chem., Int. Ed.*, 2020, **59**, 18586–18590.
- 4 G. Kummerlöwe, I. Balteanu, Z. Sun, O. P. Balaj, V. E. Bondybey and M. K. Beyer, *Int. J. Mass Spectrom.*, 2006, **254**, 183–188.
- 5 C. Adlhart and E. Uggerud, *Chem. Commun.*, 2006, 2581–2582.
- 6 U. Achatz, C. Berg, S. Joos, B. S. Fox, M. K. Beyer, G. Niedner-Schatteburg and V. E. Bondybey, *Chem. Phys. Lett.*, 2000, **320**, 53–58.
- 7 C. Adlhart and E. Uggerud, *Chem. – Eur. J.*, 2007, **13**, 6883–6890.
- 8 S. M. Lang, A. Frank and T. M. Bernhardt, *J. Phys. Chem. C*, 2013, **117**, 9791–9800.
- 9 C. A. E. Uggerud, *J. Chem. Phys.*, 2005, **123**, 214709.
- 10 P. B. Armentrout, S. E. J. Kuijpers, O. V. Lushchikova, R. L. Hightower, G. C. Boles and J. M. Bakker, *J. Am. Soc. Mass Spectrom.*, 2018, **29**, 1781–1790.
- 11 P. B. Armentrout, L. Parke, C. Hinton and M. Citir, *Chem-PlusChem*, 2013, **78**, 1157–1173.
- 12 F.-X. Li, X.-G. Zhang and P. B. Armentrout, *Int. J. Mass Spectrom.*, 2006, **255–256**, 279–300.
- 13 O. W. Wheeler, M. Salem, A. Gao, J. M. Bakker and P. B. Armentrout, *Int. J. Mass Spectrom.*, 2019, **435**, 78–92.
- 14 P. Fayet, A. Kaldor and D. M. Cox, *J. Chem. Phys.*, 1990, **92**, 254–261.
- 15 D. M. Cox, D. J. Trevor and A. Kaldor, *J. Am. Chem. Soc.*, 1990, **112**, 3742–3749.
- 16 Y. Ren, Y. Yang, Y.-X. Zhao and S.-G. He, *J. Phys. Chem. C*, 2019, **123**, 17035–17042.
- 17 X.-G. Zhao, Z.-P. Zhao, Y.-X. Zhao and S.-G. He, *J. Phys. Chem. Lett.*, 2023, **14**, 9192–9199.
- 18 J. F. Eckhard, T. Masubuchi, M. Tschurl, R. N. Barnett, U. Landman and U. Heiz, *J. Phys. Chem. A*, 2021, **125**, 5289–5302.
- 19 J. Lengyel, N. Levin, F. J. Wensink, O. V. Lushchikova, R. N. Barnett, U. Landman, U. Heiz, J. M. Bakker and M. Tschurl, *Angew. Chem., Int. Ed.*, 2020, **59**, 23631–23635.
- 20 J. F. Eckhard, T. Masubuchi, M. Tschurl, R. N. Barnett, U. Landman and U. Heiz, *J. Phys. Chem. C*, 2018, **122**, 25628–25637.
- 21 N. Levin, J. Lengyel, J. F. Eckhard, M. Tschurl and U. Heiz, *J. Am. Chem. Soc.*, 2020, **142**, 5862–5869.
- 22 T. J. MacMahon, S. W. Buckner, G. D. Byrd and B. S. Freiser, *Inorg. Chem.*, 1989, **28**, 3511–3518.
- 23 C. S. Hinton, L. G. Parke and P. B. Armentrout, *J. Phys. Chem. C*, 2007, **111**, 17773–17787.
- 24 S. Hirabayashi and M. Ichihashi, *J. Phys. Chem. A*, 2019, **123**, 6840–6847.
- 25 S. Shin, P. B. Armentrout and R. Liyanage, *J. Phys. Chem. A*, 2006, **110**, 1242–1260.
- 26 A. Simon, J. Lemaire, P. Boissel and P. Maître, *J. Chem. Phys.*, 2001, **115**, 2510–2518.
- 27 K. K. Irikura and J. L. Beauchamp, *J. Am. Chem. Soc.*, 1991, **113**, 2769–2770.
- 28 N. Aristov and P. B. Armentrout, *J. Phys. Chem.*, 1987, **91**, 6178–6188.
- 29 H. Zhang, H. Wu, Y. Jia, B. Yin, L. Geng, Z. Luo and K. Hansen, *Commun. Chem.*, 2020, **3**, 148.
- 30 Z. Yuan, Y.-X. Zhao, X.-N. Li and S.-G. He, *Int. J. Mass Spectrom.*, 2013, **354–355**, 105–112.
- 31 Z. Yuan, Z.-Y. Li, Z.-X. Zhou, Q.-Y. Liu, Y.-X. Zhao and S.-G. He, *J. Phys. Chem. C*, 2014, **118**, 14967–14976.
- 32 X.-N. Wu, B. Xu, J.-H. Meng and S.-G. He, *Int. J. Mass Spectrom.*, 2012, **310**, 57–64.
- 33 M. J. Frisch, G. W. Trucks, H. B. Schlegel, G. E. Scuseria, M. A. Robb, J. R. Cheeseman, G. Scalmani, V. Barone, B. Mennucci, G. A. Petersson, H. Nakatsuji, M. Caricato, X. Li, H. P. Hratchian, A. F. Izmaylov, J. Bloino, G. Zheng, J. L. Sonnenberg, M. Hada, M. Ehara, K. Toyota, R. Fukuda, J. Hasegawa, M. Ishida, T. Nakajima, Y. Honda, O. Kitao, H. Nakai, T. Vreven, J. A. Montgomery Jr, J. E. Peralta, F. Ogliaro, M. Bearpark, J. J. Heyd, E. Brothers, K. N. Kudin, V. N. Staroverov, R. Kobayashi, J. Normand, K. Raghavachari, A. Rendell, J. C. Burant, S. S. Iyengar, J. Tomasi, M. Cossi, N. Rega, J. M. Millam, M. Klene, J. E. Knox, J. B. Cross, V. Bakken, C. Adamo, J. Jaramillo, R. Gomperts, R. E. Stratmann, O. Yazyev, A. J. Austin, R. Cammi, C. Pomelli, J. W. Ochterski, R. L. Martin, K. Morokuma, V. G. Zakrzewski, G. A. Voth, P. Salvador, J. J. Dannenberg, S. Dapprich, A. D. Daniels, Ö. Farkas, J. B. Foresman, J. V. Ortiz, J. Cioslowski and D. J. Fox, *Gaussian 09, Revision A.01*, Gaussian, Inc., Wallingford, CT, 2009.
- 34 C. Lee, W. Yang and R. G. Parr, *Phys. Rev., B Condens. Matter*, 1988, **37**, 785–789.
- 35 A. D. Becke, *J. Chem. Phys.*, 1993, **98**, 5648–5652.
- 36 A. Schäfer, C. Huber and R. Ahlrichs, *J. Chem. Phys.*, 1994, **100**, 5829–5835.
- 37 X.-L. Ding, Z.-Y. Li, J.-H. Meng, Y.-X. Zhao and S.-G. He, *J. Chem. Phys.*, 2012, **137**, 214311.
- 38 H. B. Schlegel, *J. Comput. Chem.*, 1982, **3**, 214–218.
- 39 C. Gonzalez and H. B. Schlegel, *J. Chem. Phys.*, 1989, **90**, 2154–2161.
- 40 E. D. Glendening, J. K. Badenhoop, A. E. Reed, J. E. Carpenter, J. A. Bohmann, C. M. Morales and F. Weinhold, *NBO 5.9*, Theoretical Chemistry Institute, University of Wisconsin, Madison, WI, 2009.
- 41 J. Roithová and D. Schröder, *Chem. Rev.*, 2010, **110**, 1170–1211.
- 42 R. Wesendrup, C. Heinemann and H. Schwarz, *J. Phys. Chem. A*, 1995, **239**, 75–83.
- 43 S. Zhou, J. Li, M. Schlangen and H. Schwarz, *Angew. Chem., Int. Ed.*, 2016, **55**, 10877–10880.

- 44 K. K. Irikura and J. L. Beauchamp, *J. Am. Chem. Soc.*, 1989, **111**, 75–85.
- 45 K. Chen, Z.-C. Wang, M. Schlangen, Y.-D. Wu, X. Zhang and H. Schwarz, *Chem. – Eur. J.*, 2011, **17**, 9619–9625.
- 46 I. Kretschmar, A. Fiedler, D. Schröder and H. Schwarz, *J. Am. Chem. Soc.*, 1996, **118**, 9941–9952.
- 47 A. Fiedler, M. F. Ryan, D. Schroeder and H. Schwarz, *J. Am. Chem. Soc.*, 1995, **117**, 2033–2040.
- 48 H. Schwarz, D. Schröder, D. E. Clemmer, Y. Chen, P. B. Armentrout and V. I. Baranov, *Int. J. Mass Spectrom. Ion Processes*, 1997, **161**, 175–191.
- 49 A. Fiedler, M. F. Ryan, D. Schroeder and H. Schwarz, *Organometallics*, 1994, **13**, 4072–4081.
- 50 A. Božović, S. Feil, G. K. Koyanagi, A. A. Viggiano, X. Zhang, M. Schlangen, H. Schwarz and D. K. Bohme, *Chem. – Eur. J.*, 2010, **16**, 11605–11610.
- 51 N. Dietl, C. van der Linde, M. Schlangen, M. K. Beyer and H. Schwarz, *Angew. Chem., Int. Ed.*, 2011, **50**, 4966–4969.
- 52 L. Yue, S. Zhou, X. Sun, M. Schlangen and H. Schwarz, *Angew. Chem., Int. Ed.*, 2018, **57**, 3251–3255.
- 53 G. Logothetis and P. L. A. Popelier, *J. Organomet. Chem.*, 1998, **555**, 101–111.
- 54 M. Brookhart, M. L. H. Green and G. Parkin, *Proc. Natl. Acad. Sci. U. S. A.*, 2007, **104**, 6908–6914.
- 55 L. Lin, D. M. Spasyuk, R. A. Lalancette and D. E. Prokopchuk, *J. Am. Chem. Soc.*, 2022, **144**, 12632–12637.
- 56 L. Andrews, H.-G. Cho and X. Wang, *Angew. Chem., Int. Ed.*, 2004, **44**, 113–116.
- 57 M. Lein, *Coord. Chem. Rev.*, 2009, **253**, 625–634.
- 58 N. Berkaine, P. Reinhardt and M. E. Alikhani, *Chem. Phys.*, 2008, **343**, 241–249.
- 59 K. M. Altus and J. A. Love, *Commun. Chem.*, 2021, **4**, 173.